Experimental and Numerical Investigation of Secondary Flow Structures in an Annular LPT Cascade under Periodical Wake Impact

Martin Sinkwitz, Benjamin Winhart, David Engelmann, Francesca Di Mare, Ronald Mailach

▶ **To cite this version:**

Martin Sinkwitz, Benjamin Winhart, David Engelmann, Francesca Di Mare, Ronald Mailach. Experimental and Numerical Investigation of Secondary Flow Structures in an Annular LPT Cascade under Periodical Wake Impact: Part 1: Experimental Results. 17th International Symposium on Transport Phenomena and Dynamics of Rotating Machinery (ISROMAC2017), Dec 2017, Maui, United States. hal-02980961

HAL Id: hal-02980961
https://hal.science/hal-02980961

Submitted on 27 Oct 2020

HAL is a multi-disciplinary open access archive for the deposit and dissemination of scientific research documents, whether they are published or not. The documents may come from teaching and research institutions in France or abroad, or from public or private research centers.

L'archive ouverte pluridisciplinaire **HAL**, est destinée au dépôt et à la diffusion de documents scientifiques de niveau recherche, publiés ou non, émanant des établissements d'enseignement et de recherche français ou étrangers, des laboratoires publics ou privés.

Distributed under a Creative Commons Attribution 4.0 International License

Experimental and Numerical Investigation of Secondary Flow Structures in an Annular LPT Cascade under Periodical Wake Impact – Part 1: Experimental Results

Martin Sinkwitz[1]*, Benjamin Winhart[1], David Engelmann[1], Francesca di Mare[1], Ronald Mailach[2]

ISROMAC 2017

International Symposium on Transport Phenomena and Dynamics of Rotating Machinery

Maui, Hawaii

December 16-21, 2017

Abstract

Experimental studies have been conducted on a modified T106 low pressure turbine (LPT) profile in a 1.5 stage annular axial turbine rig at the Chair of Thermal Turbomachines, Ruhr-Universität Bochum. The rig setup allows the highly resolved measurement of unsteady wake-stator flow interaction in both space and time. Incoming wakes are generated by a variable-speed driven rotor equipped with cylindrical bars.

In the present paper an experimental approach to the investigation of unsteady phenomena is proposed. Time-averaged as well as instantaneous measurement data from 2D flow field traverses at the stator exit are provided for the analysis of the periodically unsteady vortex formation, displacement and suppression. Additional time-accurate blade pressure data is used to study the relationship between the detected secondary flow downstream of the stator row and the immediate wake impact on the blade profile.

Keywords

Axial Turbomachinery — Secondary Flow — Wakes — Unsteady Flow Measurements

[1] *Chair of Thermal Turbomachines, Ruhr-Universität Bochum, Bochum, Germany*

[2] *Chair of Turbomachinery and Flight Propulsion, Technische Universität Dresden, Dresden, Germany*

***Corresponding author**: Martin.Sinkwitz@rub.de

INTRODUCTION

Blade count reduction in the low pressure part of the aero engine can provide a substantial contribution to the reduction of the overall weight of an engine. However, this must be compensated through the design of high-lift, heavy-loaded blades which in turn are exposed to increased pressure gradients, affecting in particular blade profile and end wall flow which is already prone to separation. Intensified boundary layer separation at end walls and on the profile suction side results in pronounced secondary flow systems. These in turn induce high loss, a loss of lift and main flow perturbation [1, 2]. Different secondary flow models have been proposed, extended and modified, resulting in a basic, broadly accepted, secondary flow model representation (e.g. [2]). This concept mainly consists of passage vortices (PV), horse shoe vortices (HSV), tip leakage vortex, corner vortices (CV) and a vortex street that is shed from the blade trailing edge (TEWV). A few of the models incorporate yet another vortex structure originating from the separated suction side boundary layer, labeled as the concentrated shed vortex (CSV) [3], resulting from end wall boundary layer fluid (PV) impinging on the blade suction side and leading to a separation of the suction side boundary layer itself close to the end wall. Analysis and potential reduction of these vortical structures are complicated by the multistage environment in turbomachines, where rotor stator interaction affects the transport and shedding of blade wakes and vortices, resulting in an extremely non-uniform, distorted and time-dependent flow field. Thus, it is difficult to separate the distinct interacting flow structures from each other and to determine their degree of influence on aerodynamic loss generation mechanisms. Numerous tests have been conducted under simplified conditions in linear cascades. To include the influence of periodically unsteady rotor blade wakes in linear setups, linear wake generators have been employed, using cylindrical bars to simulate wakes [3, 4, 5, 6, 7, 8, 9, 10]. An important common finding of these investigations is that unsteady wake inflow can stabilize boundary layer flow. Thus, periodic reattachment of a boundary layer, which would separate under unperturbed inflow conditions, is promoted [8, 9, 11]. However, the investigation of secondary flow within linear cascades neglects several essential effects present in real turbomachinery flow.

In this study an experimental setup for the time-resolved analysis of wake-stator flow interaction, using an annular geometry instead of a linear cascade, is applied. This way, the influence of curvilinear end walls, non-uniform, radially increasing pitch and radial flow migration is incorporated. Incoming wakes are generated by a variable-speed driven rotor disk equipped with cylindrical bars. Special emphasis is put on wake-induced, time-dependent weakening and dis-

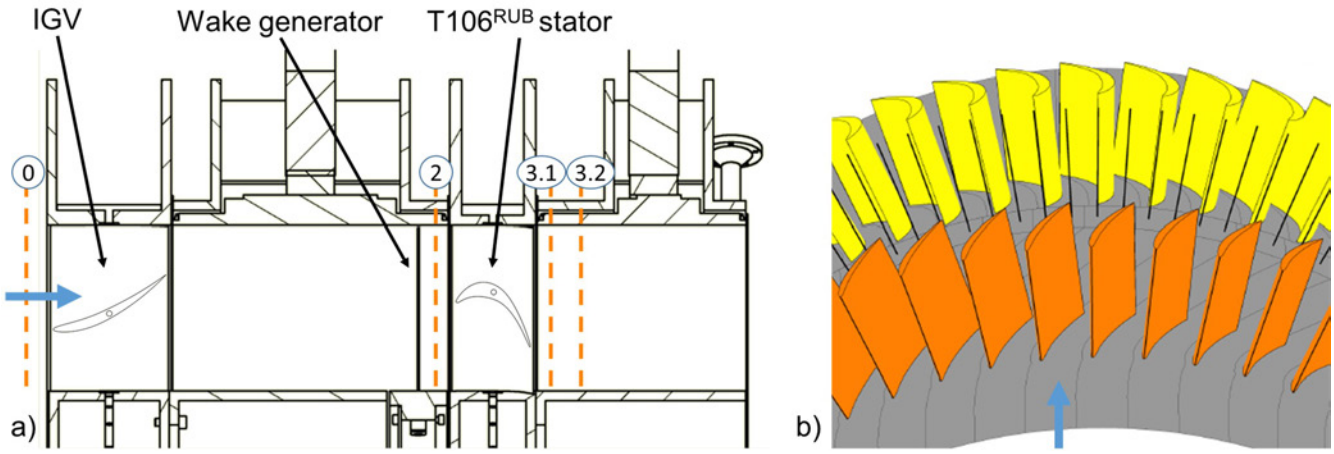

Figure 1. Experimental Test Facility. Sectional view (a), 3D illustration (b).

placement of particular vortices of the secondary flow system. Furthermore, wake-boundary layer flow interaction and flow separation along the blade suction surface is studied. The distinction between time-averaged and time-resolved analysis of secondary flow phenomena and the importance of time-resolved measurement is emphasized and the temporal evolution of characteristic flow field quantities is utilized to analyze the periodic impact on the vortices. By relating measurement data of two-dimensional flow field traverses and time-accurate blade profile pressure signals to each other, a deeper understanding of the complex interaction between bar wake, boundary layer and secondary flow can be obtained.

1. EXPERIMENTAL TEST FACILITY

For this study an existing large scale axial flow turbine test rig installed at the Chair of Thermal Turbomachines of Ruhr-Universität Bochum was retrofitted to allow highly resolved measurements of unsteady wake-stator flow interaction. Pivot-mounted casing elements with multiple probe accesses have been constructed which are placed between the IGV and the stator row as well as downstream of the stator. Stepwise rotation of these elements and radial translation of the probes enable the automated recording of two-dimensional flow traverses. The test facility is operated continuously in an open circuit, with ambient air. Flow is induced by a 150 kW variable speed engine coupled to a radial blower with a $\dot{m}$ = 13 kg/s mass flow capacity. The blower is placed downstream of the test section, so that the rig is operated in suction mode. The large dimensions of the flow channel allow detailed flow measurements with negligible blockage and perturbation by installed probes.

The aft-loaded blade profile under investigation, labeled as T106^{RUB}, is an in-house modification of the well-known T106 LPT blade. It was developed for matching the characteristics of the T106 profile at the rig's low Mach number flow. The development and underlying principles of the transformation procedure are described in [12]. The profile is characterized by a cylindrical geometry with a chord length of C = 0.1 m and an aspect ratio of H/C = 1.7. This aspect ratio ensures that near end wall vortices do not merge and as a consequence quasi two-dimensional flow conditions at mid-span. The stator row consists of 60 blades with a stagger angle of λ_{T106} = 30.7° and a pitch-to-chord ratio at mid-span of g/C = 0.78.

An inlet guide vane (IGV) row ensures proper inflow angles to the stator. It is made up of 60 vanes (NACA 8408 profile) and was developed for correct flow turning whilst leaving the T106^{RUB} inflow as far as possible unaffected by wakes and secondary flow structures. The choice of 60 NACA 8408 profiles is the result of an elaborate numerical study, comparing 42 different profile geometries and several blade counts. The IGV is placed 2.61 C upstream of the bar plane utilizing the maximal possible distance the axial test rig dimensions allowed.

To simulate blade wakes, the rotor disk was equipped with radially stacked steel bars (bar diameter D_B = 0.002 m, bar length L_B = 0.168 m, bar pitch g_B = 0.039/0.078/0.117 m). Thus, it is possible to isolate both velocity defect and turbulence increase of rotor blade wakes without the additional secondary flow system, associated with flow turning in a blade passage. Wakes are generated in a plane parallel to the stator leading edges (LE), located at an axial distance of 0.33 C upstream of the LE, which represents a typical axial gap width in a LPT. The investigations were carried out for three different values of bar pitch. The same stator and IGV blade counts (60) as well as the number of wake generator bars (40/60/120) allow time-efficient numerical studies.

A 15 kW AC engine controlled by a frequency converter drives the rotor shaft. The setup of IGV, wake generator and T106^{RUB} stator is shown in Figure 1.

2. MEASUREMENT TECHNIQUES

Adjustment and monitoring of the operating point was realized with help of multiple Prandtl-probes (p_t, p_s and hence c) at different characteristic planes, a stationary five hole probe (5HP) (p_t, p_s, c, flow angles α and γ) in the stator exit and a combined temperature and relative humidity sensor at the test rig inlet. The ambient pressure (reference pressure, abso-

lute) was measured by a Rosemount 3051 absolute pressure transducer (accuracy ±0.15 % of calibrated transducer measuring range). All remaining pressures (relative to ambient) were recorded by a 64-channel Scanivalve ZOC33/64Px miniature pressure scanner module (accuracy ±0.10 % of transducer full-scale range) controlled by a Scanivalve ERAD4000 unit. The 64 individual high-sensitivity low-range (70 mbar) pressure sensors enable simultaneous data acquisition of all incorporated pneumatic pressure probes. By recording pressures practically without temporal offset between one and another, the systematic measurement uncertainty – e.g. of 5HP, wall or profile pressure measurements - is reduced considerably.

Table 1. Main geometric test rig properties and turbine stage parameters

Test rig		
Outer diameter (Casing)	D_C	1.660 m
Inner diameter (Hub)	D_H	1.320 m
Mid-span diameter	D_m	1.490 m
Turbine stage		
Blade height IGV, T106^{RUB}	H	0.170 m
Chord length IGV	C_{IGV}	0.137 m
Stagger angle IGV	λ_{IGV}	-25.5°
Chord length T106^{RUB}	C_{T106}=C	0.100 m
Stagger angle T106^{RUB}	λ_{T106}	30.7°
Blade count IGV, T106^{RUB}	$n_{IGV,T106}$	60
Design flow angles, mid-span:		
IGV inlet	α_0	90.0°
IGV outlet = T106^{RUB} inlet	α_1=α_2	52.3°
T106^{RUB} outlet	α_3	153.2°
Axial distances:		
IGV TE - bar plane	x/C_{T106}	2.61
bar plane - T106^{RUB} LE	x/C_{T106}	0.33
Bar diameter	D_B	0.002 m
Bar length	L_B	0.168 m
Bar pitch at mid-span	g_B	0.039 m, 0.078 m, 0.117 m
Operating point, Design point		
Mass flow	$\dot{m}$	12.8 kg/s
Reynolds number (exit, th.)	$Re_{exit,\,th}$	200,000
Mach number (exit, th.)	$Ma_{exit,\,th}$	0.091
Strouhal number range	Sr	0.45–3.15
Flow coefficient range	ϕ	0.81–2.84

For this study, two-dimensional (2D) (in radial and circumferential direction) flow field traverses have been carried out downstream of stator TE (Figure 1, plane 3.1) to quantify the bar wake impact on the downstream secondary flow system. For time-averaged traverses, miniature 5HP (head diameter of 2 mm, bore diameter of 0.3 mm) were employed. Hot wire anemometry measurements (CTA mode) provided time-resolved traverse data. For acquisition of the time-resolved 3D flow vector these were conducted with two different types of Split Fiber Probes (SFP), fabricated by Dantec Dynamics. SFP probes of type 55R56 were used for measuring axial and radial velocity components (for computing flow angle δ) and probes of type 55R57 for measuring axial and circumferential components (for computing flow angle α). Hot wire signals have been recorded at a rate of 50 kHz (125 times higher than the maximum bar passing frequency) for at least 50 samples, triggered by a one/revolution signal from an inductive encoder on the rotor shaft. The minimum of 50 samples was defined as the best trade-off between time consumption (of 2D traverses) and validity of the phase-averaged results. For the discussed investigations, where unsteady fluctuations in the wake flow exceed the angular range of ±45° and where recording rates of 50 kHz are sufficient, SFP have shown superior performance over conventional X-array probes. As 3D SFP are not available and conventional triple-sensor wire-probes are too large in diameter for the test rig probe accesses, acquisition of all three velocity components requires the combined use of the two different types of SFP. Measurement data of both probes were correlated and post-processed to obtain 3D flow vectors. For SFP data acquisition a StreamLine 90N10 CTA anemometer by Dantec Dynamics (incorporating three 90C10 CTA modules) in combination with a National Instruments NI 9215 A/D converter was employed. High spatial traverse resolution was achieved by 2D measurement grids of up to 46 radial and 49 circumferential positions. The circumferential positions were evenly distributed over two stator pitches, whereas the radial increments were refined close to the end walls. In the case of time-consuming SFP-measurements the spatial resolution was decreased slightly. At the start of every measurement, probes were aligned to the main flow direction at mid-span. 5HP measurements were carried out with fully calibrated probes in a non-nulling mode.

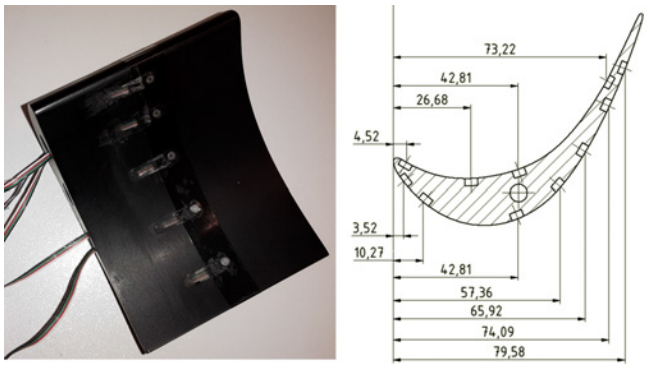

Figure 2. T106^{RUB} blade, instrumented with Kulite LQ-125 sensors for time-resolved profile pressure measurements. Pressure side view (left) and arrangement of sensors (right).

For additional data acquisition within the T106^{RUB} stator passage, blade profile pressures were measured on various T106^{RUB} stator blades. 84 pressure taps, evenly distributed to 3 positions of constant span (near hub at R/H = 10 %, at

mid-span at R/H = 50 %, near casing at R/H = 90 %) enabled time-averaged, pneumatic pressure measurement. Furthermore, time-resolved, piezo-electric pressure measurements were conducted at mid-span, using 10 flush-mounted Kulite type LQ-125 sensors (see Figure 2). An IMC CRONOSflex system was incorporated for recording Kulite signals with an acquisition rate of 50 kHz. At every measurement position 200 samples were collected, also triggered once per revolution. A phase-locked ensemble averaging technique was applied to the recorded time-resolved data samples to obtain reliable quantities from SFP and Kulite sensor measurements. This facilitates the separation of periodically unsteady signals originating from wake impact from stochastic turbulent fluctuations without losing the time-dependent character. All shown time-resolved results have been averaged with this method.

3. EXPERIMENTAL RESULTS AND DISCUSSION

For all investigations discussed in this paper, the theoretical exit Reynolds number was kept constant at $Re_{\text{exit, th}}$ = 200,000 (based on T106$^{\text{RUB}}$ chord length C, with the fluid's dynamic viscosity μ, the theoretical exit velocity $c_{\text{exit, th}}$ and the corresponding density $\rho_{\text{exit, th}}$):

$$Re_{\text{exit, th}} = \frac{c_{\text{exit, th}} \cdot \rho_{\text{exit, th}} \cdot C}{\mu} \tag{1}$$

This is a typical value for LPT operation at high altitude where suction side boundary layer separation can occur. The theoretical exit state (using upstream total pressure and downstream static pressure) is a common way to account for altered losses when bar velocity or bar count are modified while maintaining comparability. As the main dimensionless quantities for characterizing unsteady flow disturbances, the Strouhal number Sr and flow coefficient ϕ have been identified [6, 12]:

$$Sr = f_{\text{BP}} \cdot \frac{C}{c_{\text{ax}}} = \frac{c_{\text{B}}}{g_{\text{B}}} \cdot \frac{C}{c_{\text{ax}}} \tag{2}$$

$$\phi = \frac{c_{\text{ax}}}{c_{\text{B}}} \tag{3}$$

To study the effect of different periodically unsteady inflow conditions (disturbance by incoming wakes), these have been varied in wide ranges including values for typical LPT operation. As for all discussed measurements the axial velocity c_{ax} is approximately held constant, bar wake frequency f_{BP} and thus Sr and ϕ were modified by altering bar speed c_{B} and/or bar pitch g_{B}. The results presented in this article are based on findings from previous work by the authors [12] where detailed analysis of 2D flow field traverses were conducted for different combinations of Sr and ϕ. By including time-resolved blade pressure data for the present work, a causality relationship between the blade passage and downstream flow can be established.

3.1 Stator exit flow

2D flow field traverses have been conducted in multiple planes downstream of the T106$^{\text{RUB}}$ stator row. Measurement data from these planes permit an evaluation of the secondary flow system emerging upstream within the stator passage. By comparing flow fields of different stator exit flow planes, the processes based on the mixing of stator wakes and vortices with the free passage flow can be described. By considering different operating points - defined by combinations of Sr and ϕ - and comparing them with the unperturbed case, the effect of bar wakes and the temporal evolution of secondary flow structures can be derived (for detailed underlying analysis see [12]).

3.1.1 Time-averaged measurement data

Figure 3 shows time-averaged (obtained with 5HP) distributions of axial vorticity (AVO) in plane 3.1 (Figure 1a), 0.15 C downstream of stator TE in the range of two stator pitches.

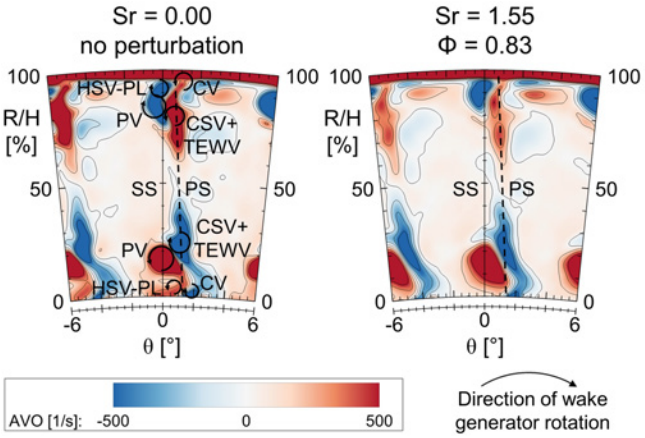

Figure 3. Time-averaged results 0.15 C downstream of TE. AVO distribution for steady undisturbed case (left) and for a case with significant wake disturbed inflow (Sr = 1.55, ϕ = 0.83) (right).

The AVO can be derived from those components of the velocity vector, tangential to the axial direction (c_{y} and c_{z}) and the geometry of the measurement grid:

$$AVO = \frac{\partial c_{\text{z}}}{\partial y} - \frac{\partial c_{\text{y}}}{\partial z} \tag{4}$$

The flow field is given for the undisturbed (left) and a perturbed (right) case, whereas the direction of view is upstream. Relevant vortices of the stator secondary flow system, the estimated stator wake position as well as the position of suction and pressure side of the stator wake have been labeled to aid interpretation. The particular vortices have been identified by their direction of rotation and their location in the vicinity of characteristic flow regions, such as the suction side or the end walls. Thus, the passage vortex (PV) pair could be detected near the end walls on the suction side of the stator wake. The PV pair is a result of low momentum end wall boundary layer fluid, following the cross passage

pressure gradient from the pressure side to the suction side of the neighboring blade. Impinging at the profile suction side, this crossflow is diverted across the blade towards mid-span, consequently shaping the PV. Furthermore, near the profile LE the horse shoe vortex (HSV) system is formed, when the end wall boundary layer from upstream hits the LE and splits due to the local adverse pressure gradient. The suction side legs (HSV-SL) propagate close to the suction side as they are pushed against the blade by the cross passage pressure gradient. As the suction side legs are concentrated within the corner between end wall and blade suction side, they do not contain much material, stay small and potentially merge with the respective nearby corner vortex (CV). The pressure side legs (HSV-PL), instead, are diverted from the blade pressure side to the suction side of the adjacent blade, also following the cross passage pressure gradient. For the steady, unperturbed case the HSV-PL can clearly be identified among the PV and the respective end wall. Despite the same direction of rotation, these have not merged entirely with the PV, as reported for other setups e.g. in [2, 10]. Instead they push the PV towards mid-span. In close proximity, a spacious system can be detected, rotating in opposite direction. This system is supposed to contain the concentrated shed vortex (CSV), the described combination of CV and HSV-SL, as well as the trailing edge wake vortex street (TEWV). The origin of the CSV is a direct consequence of the low momentum PV flow impinging at the blade suction side. It induces separation of the suction side boundary layer, which then rolls up into a counter rotating vortex next to the PV [12]. At TE the adverse directions of radial blade flow migration on pressure and suction side form a shear layer (TEWV) that unites with the CSV.

In the right part of Figure 3, with $Sr = 1.55$, $\phi = 0.83$ a case with significant periodical inflow perturbation is displayed. In direct comparison with the unperturbed case an apparent impact on several vortical structures can be observed. Near the casing both a decrease in size and a displacement of the PV + HSV-PL system towards the end wall can be seen. Furthermore, a significant weakening of the CSV + TEWV takes place. This can be justified by the impact of the bar wakes, which interact with boundary layer flow on the blade and on end walls. The wakes, acting as negative jets, promote boundary layer transition and leave the wall flow in a temporarily unperturbed condition after the wake has passed [11, 12, 13]. In this state the boundary layer is not as prone to separation and deflection as in the undisturbed case. Intermittently, cross passage transport of end wall flow is reduced and less low momentum fluid is provided to the PV, reducing its dimensions. Further on, separation of boundary layer flow at the profile suction side is periodically reduced, as well. As a consequence, particularly the CSV is weakened, as it results from boundary layer material both from the end wall and from the profile suction side. Near the hub, impact on the secondary flow system seems slightly different. The PV appears even larger, but also more diluted. A weakening of the CSV+TEWV system is observable, but not as pronounced as near the casing. Thus inspection of the time-averaged exit flow field already indicates the spatial imbalance (hub/casing) of bar wake impact in an annular cascade contrary to the uniform flow in linear cascades.

3.1.2 Time-resolved measurement data

For a more detailed insight into the intermittent flow phenomena downstream of the $T106^{RUB}$ stator passage, time-accurate data were recorded with SFP. The probes were traversed similarly to 5HP measurements in the same plane 0.15 C downstream of stator TE. Three observation stations have been selected at various spanwise positions (R/H = 20 %, 50 %, 85 %) and the corresponding flow field temporal evolution over three bar passing periods of c and AVO are represented in Figure 4. The stations capture the secondary flow systems near the hub and the shroud and the flow at mid-span. The operating point ($Sr = 1.55$, $\phi = 0.83$) matches the one chosen in Figure 3 (right). Thus, Figure 3 (right) represents the time-averaged picture of the time-resolved phenomena depicted in Figure 4.

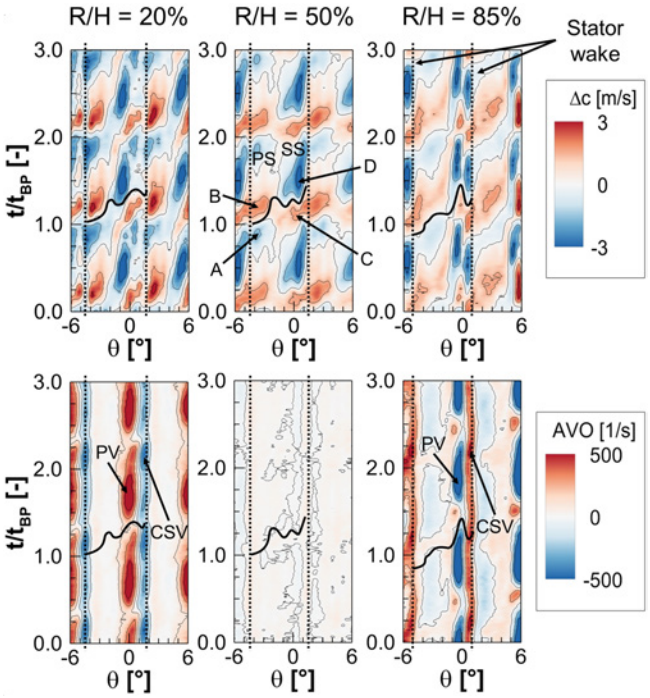

Figure 4. Time-resolved results 0.15 C downstream of TE. Time-space evolution of Δc (top) and AVO (bottom) for three slices at constant span, $Sr = 1.55$, $\phi = 0.83$.

In the upper part of Figure 4 the temporal evolution of velocity c is given, in the lower the same can be seen for the AVO. For the velocity evolution, the respective local values at undisturbed condition have been subtracted from the time-resolved, phase-averaged velocity values:

$$\Delta c\,(R, \theta, t) = c\,(R, \theta, t) - c\,(R, \theta)_{\text{steady}} \tag{5}$$

For the AVO, absolute values are shown. Approximate locations of the stator wakes have been marked with dotted

vertical lines, also suction side (SS) and pressure side (PS) flow. The velocity field is perturbed periodically with the bar (wake) passing frequency ($t_{BP} = 1/f_{BP}$ correlates to the duration of one bar passing). However, the situation that can be observed downstream of the stator is not just a periodical perturbation by the passing bar wake, but a superposition of several effects, which can be traced back to wake kinematics and the displacement of vortices. While propagating through the stator passage, the incoming bar wakes are cut, stretched, bowed, undergo mixing and interact with the passage flow as well as with the near wall flow at the blade suction and pressure side and at the end walls. The bar wakes, acting as local regions of low pressure, momentum and velocity can be described as negative jets [11, 14], pointing in the opposite direction than the main flow. When impinging on the profile pressure side and passing over it, the bar wake induces two counter rotating, vortical-like structures (radial rotational direction) (compare e.g. [13] or [15]). This results in a flow deceleration in front of the wake and a flow acceleration immediately after the wake has passed. On the suction side the impact on flow is reversed. Here, the wake pushes a region of accelerated squeezed passage flow in front of it and is followed by a low-speed region. This interaction between bar wake and profile flow will be discussed in more detail in section 3.2 and in [15]. The described local flow acceleration and deceleration within the stator passage finally result in four characteristic, periodically passing parcels of altered velocity that can still be observed in the stator exit flow field. For the flow at mid-span (R/H = 50 %) these four parcels close to the bar wake have been labelled with A-D in Figure 4 (top center). The distorted bar wakes have been highlighted, as well. Immediately before the wake arrives, decelerated volume A and accelerated volume C are present. When the bar wake has passed the observed plane, parcels B and D follow. Based on their origin, these four volumes are located near the blade suction and pressure side respectively and thus close to the stator profile wakes. Consequently, especially close to the profile wake a pulsating flow field is induced, whereas the free passage flow is little disturbed. Downstream of the passage, the accelerated parcels B and C from previously separated, adjacent passages merge. Interestingly, there is nearly no change at all regarding the AVO (bottom center), remaining fairly constant over time, indicating that no additional vortices with axial sense of rotation are generated. This corresponds to the observation that the vortical structures, induced by the negative jet like propagation of the bar wake, generate vortices with primary radial rotational direction.

Near the end walls, the situation is far more complex than at mid-span. Beyond the pulsating bar wake impact, the flow field here is affected by the stator secondary flow structures. Both at R/H = 20 % and R/H = 85 % the velocity distributions undergo a similar periodical perturbation as already described for the flow at mid-span. But although the characteristic parcels can be found again, an apparent difference is noticed regarding structures C and D, as they are broken up and displaced from the suction side into the passage. This can be traced back to the periodical interaction between bar wake and the nearby secondary flow system. It has to be noted that the altered velocity is a result both of the passing bar wake velocity field and of displaced vortical structures carrying low velocity fluid. By including the evolution of the AVO into the analysis, this interaction can be observed more clearly. In the range of -0.5° ≤ θ ≤ 0.5° a periodical weakening of the PV (within the regarded plane) becomes visible. This weakening can be linked to the approaching bar wake carrying the accelerated flow regime C. When the wake has passed, the decelerated structure D is split, as is wraps around the PV. At the same time, the nearby CSV ($\theta \approx 1.5°$) is periodically weakened as well. As the comparison with adjacent spanwise slices (below and above, not shown here) has revealed, additionally to the intermittent weakening and strengthening of PV and CSV, they are also displaced radially. Both weakening as well as radial displacement out of the observed plane reduce the local magnitude of the AVO. As the CSV is far more displaced (in radial direction) than the PV, its core is intermittently located within the observed plane, above or below. This wavelike in-and-out of plane movement must not be misinterpreted as a pattern occurring at a doubled frequency. The influence on the secondary flow structures in turn can be traced back to a combination of a direct and an indirect bar wake impact. When the bar wake passes, its local velocity field (parcels A-D) has a direct impact on the exit flow field including the secondary flow system. Additionally, the vortex development has already been affected upstream by the bar wake passing through the stator passage, but back in time. As only the temporal offset consequences of this effect can be observed in the exit flow, the authors term this the indirect impact. Based on the interaction between the bar wake (periodical altered velocity field and injection of momentum and turbulence) and the flow through the passage near the end walls, the cross passage transport is decreased and vortex formation and propagation are seriously influenced. The authors assume, that initially the propagation of the HSV-PL is massively perturbed by the passing wakes. Its impingement position at the adjacent blade suction side is shifted downstream, reducing impact on suction side flow and thus on PV and CSV. Under unperturbed inflow both PV and CSV are pushed towards mid-span by the intense HSV-PL. Under wake impact, they are periodically shifted back towards the end wall. Due to slower propagation of the vortical secondary flow structures than the main flow, the effects of passing bar wake (direct) and affected secondary flow structures (indirect) arrive at different instants of time in the observed plane in the stator exit flow. Furthermore, the different propagation velocities at mid-span, hub and casing also induce a temporal shift between the impact of the bar wakes at different spanwise positions.

3.2 Profile pressure distribution

Evaluation of the stator exit flow field allows an analysis of bar wake-secondary flow interaction. To examine the immediate impact of periodically unsteady bar wakes on stator blade profile flow, experimental data from within the

passage is necessary. Thus, multiple positions on various T106^{RUB} stator blades were equipped with pressure taps. At first, time-averaged, pneumatic pressure readings will be discussed, followed by time-accurate measurement data from piezoelectric sensors, embedded in the blade surfaces.

3.2.1 Time-averaged measurement data

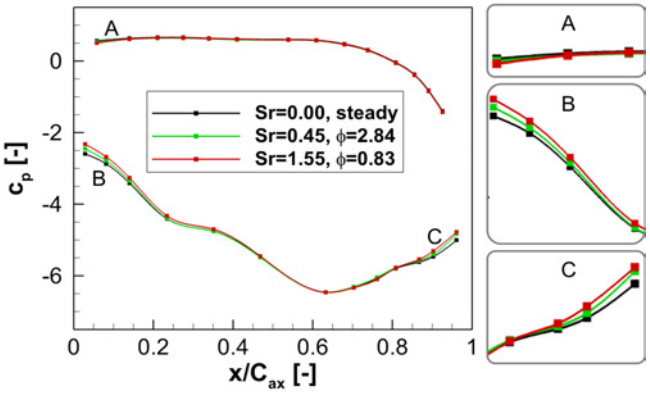

Figure 5. Time-averaged c_p distributions at T106^{RUB} mid-span for three different operating points.

Figure 5 shows time-averaged, non-dimensionalized static blade pressure distributions (c_p) at mid-span (R/H = 50 %) for different operating points, whereas c_p was defined as follows:

$$c_p = \frac{p(x) - p_1}{p_{t,1} - p_1} \tag{6}$$

For reasons of clarity, error bars have been omitted, see part 2 [15] for those values including error bars. The undisturbed steady situation is given by the black curve, the green curve (Sr = 0.45, ϕ = 2.84) shows a lightly disturbed case, whereas the red curve (Sr = 1.55, ϕ = 0.83) represents the already introduced case with heavy disturbance. The disturbed operating points exhibit constant bar pitch (g_B = 0.078 m) but differing bar speed and thus wake frequency. At first sight the distributions are very similar and do not feature any striking differences. On closer examination, variations confined to the regions close to LE (details A and B for $0 \leq x/C_{ax} \leq 0.2$) and close to TE (detail C for $0.8 \leq x/C_{ax} \leq 1$)) become visible. Due to the wake generator rotation closely upstream of LE, for the perturbed operating points the T106^{RUB} stator profiles experience inflow with considerable periodical incidence. As shown in prior work by the authors [12] this results in maximal deviation angles from design inflow of $\Delta\alpha$ = -9°. The negative incidence inflow shifts the stagnation point at LE towards the suction side. This decreases the velocity on the suction side (detail B) and increases it on the pressure side (detail A) close to LE. Although this is a time-accurate effect, its time-averaged impact can be observed in Figure 5. Near TE only suction side flow is influenced by the unsteady inflow (detail C). This different behavior of suction side flow near TE can possibly be traced back to the interaction between the passing bar wake and a separation bubble in the rear part of the suction side.

From comparison of these three operating points it becomes obvious that the impact of unsteady inflow on the time-averaged blade pressure distribution is very small. As a consequence, the use of pneumatic pressure taps alone giving time-averaged blade pressure distributions is not suitable for detailed analysis of the discussed unsteady phenomena.

3.2.2 Time-resolved measurement data

For deeper insight into the unsteady interaction between bar wakes and stator passage flow, time-accurate measurement data of T106^{RUB} blade pressures have been conducted. In Figure 6 the temporal evolution of local blade pressure fluctuations over two bar passing periods are given for profile flow at mid-span. Pressures on suction side ($0 \leq x/C_{ax} \leq 1$) and on pressure side ($-1 \leq x/C_{ax} \leq 0$) are shown for the two already introduced unsteady operating points with light and heavy disturbance and a third one with intermediate perturbation (Sr = 0.90, ϕ = 1.45). Similarly to equation (5), the respective values at undisturbed condition have been subtracted from the time-resolved, phase-averaged pressures.

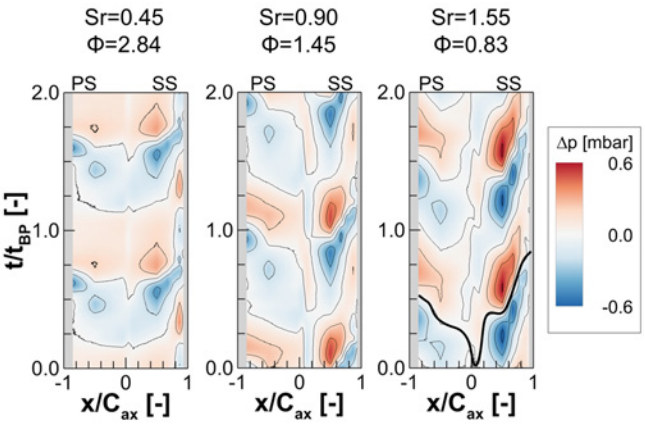

Figure 6. Time-space evolution of T106^{RUB} profile pressure fluctuations at mid-span for three periodically disturbed operating points.

For all operating points, periodical pressure fluctuations at the blade surface caused by impinging bar wakes can be observed. By analyzing the fluctuations (deviation from the undisturbed condition), the propagation of the wake disturbance from LE across suction and pressure side towards TE can be tracked. Wake kinematics, derived in the context of Figure 4, can be applied to the profile flow, as well. However, it must be noted that, as bar wake flow around one single profile is now considered in relation to the flow of multiple bar wakes through a passage of adjacent profiles (chapter 3.1.2), bar wake paths and the configuration of the induced flow structures look different. Furthermore, as static blade pressures are considered, the color scale is inverted. Parcels of high velocity correspond to decreased static pressure and vice versa. Before the bar wake impinges at LE, it wraps around it and is cut by the LE. Volume C of squeezed passage flow (high velocity and low static pressure) becomes visible at the suction side and is transported downstream towards TE. Immediately after the wake has passed, volume D (low

velocity, high static pressure) follows. This corresponds to the observations from the stator exit flow field (chapter 3.1.2).

Under low disturbance frequency (Sr = 0.45, ϕ = 2.84), the period of time between individual wake events is sufficient for blade flow to switch back to the unperturbed condition. With raising disturbance frequency and thus Sr, the amplitude of time-resolved pressure fluctuations increases significantly, reaching maximum oscillations of ±10 % (relative to cascade outlet dynamic pressure) during one bar wake passing. This results in a highly periodically unsteady blade loading under wake impact. Furthermore, for the lightly disturbed case an additional periodical oscillation can be observed close to TE ($0.8 \leq x/C_{ax} \leq 1$), pointing toward the periodical suppression of a laminar separation bubble. Under steady inflow, the suction side boundary layer is assumed to separate towards TE, forming a separation bubble. With an increasing disturbance frequency the oscillations connected to this phenomenon are reduced. This is indicative of the bubble not switching back to its undisturbed condition for sufficiently high bar wake frequencies.

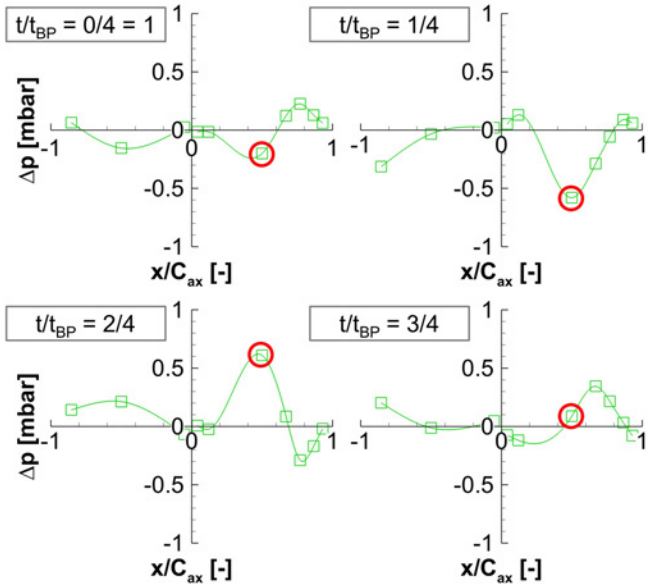

Figure 7. T106^{RUB} profile pressure fluctuations at mid-span (Sr = 1.55, ϕ = 0.83). Temporal evolution for one bar passing, divided into 4 time instants.

The impact of the passing bar wake on the profile flow can furthermore be investigated using Figure 7, showing the blade pressure fluctuations for four representative time instants of one bar wake passing, again for Sr = 1.55, ϕ = 0.83. One sensor position on the suction side (x/C_{ax} = 0.5) is highlighted with a red circle. For t/t_{BP} = 0 this position is already facing the approaching bar wake (parcel C) with decreasing pressure, which further decreases at time instant t/t_{BP} = 1/4. At t/t_{BP} = 2/4 the wake has passed and parcel D with maximum local pressure is following. For t/t_{BP} = 3/4 the wake has nearly left the profile. On the pressure side similar behavior can be recognized with lower fluctuation amplitudes.

4. CONCLUSIONS

Within the present work experimental investigations have been performed, focusing on periodically unsteady flow phenomena in a LPT stator passage of a 1.5 stage annular cascade. Conventional time-averaged measurement data is completed and combined with phase-averaged, highly time-resolved data, thus simplifying analysis within the time-domain. Through combination of flow field data in the stator exit flow and blade pressure data a link could be established between secondary flow structures downstream of the passage and underlying effects directly at the blade. The well-known secondary flow model could be applied to the stator exit flow field. Analyzing the temporal velocity and vorticity evolution in three characteristic slices of constant span, vortex displacement and weakening could be described. Furthermore, periodically unsteady structures could be identified downstream of the passage. These represent the remaining portion of the bar wakes, carrying a velocity field of four characteristic volumes of decreased and increased velocity. Finally the immediate interaction between the bar wakes and T106^{RUB} stator profile flow was presented. Similarly to observations made in the passage exit flow, on the blade suction side pressure fluctuations are enhanced considerably for the high Sr case. The interaction of bar wake and profile boundary layer flow could be characterized by the passing negative jet and its alternating sharp decrease and increase of local pressure, respectively velocity. The negative jet effect, not only describes a fluctuating velocity field, but also an injection of turbulence at various scales into the near wall flow.

ACKNOWLEDGMENTS

The investigations reported in this paper were conducted within the framework of the joint research project “Unsteady Flow and Secondary Flow in Compressor and Turbine Cascades” (PAK-530). The authors wish to gratefully acknowledge funding and support by the Deutsche Forschungsgemeinschaft (DFG). The experimental investigations would not have been possible without the efforts of our technical staff. The responsibility for the contents of this publication lies entirely by the authors.

NOMENCLATURE

Latin and Greek Symbols

c	[m/s]	velocity
c_p	[-]	non-dimensional pressure distribution
C	[m]	blade chord length
D	[m]	diameter
g	[m]	pitch (at mid-span)
H	[m]	blade height
L	[m]	length
Ma	[-]	Mach number
p	[Pa]	pressure

Latin and Greek Symbols (continued)

Re	[-]	Reynolds number
Sr	[-]	Strouhal number
t	[s]	time
x	[m]	axial direction
α	[°]	flow angle in circumferential direction
δ	[°]	flow angle in radial direction
θ	[°]	circumferential direction
λ	[°]	stagger angle
μ	[Pa·s]	dynamic viscosity of a fluid
ρ	[kg/m^3]	density of a fluid
ϕ	[-]	flow coefficient

Subscripts

ax	axial direction
B	bar
BP	bar passing
C	casing
H	hub
m	mid-span
r	radial direction
th	theoretical

Abbreviations

5HP	five hole probe
AVO	axial vorticity
CTA	constant temperature anemometry
CSV	concentrated shed vortex
CV	corner vortex
HSV	horse shoe vortex
HSV-PL	horse shoe vortex - pressure side leg
HSV-SL	horse shoe vortex - suction side leg
IGV	inlet guide vane
LE	leading edge
LPT	low pressure turbine
PS	pressure side
PV	passage vortex
SFP	split fiber probe
SS	suction side
TE	trailing edge
TEWV	trailing edge wake vortex

REFERENCES

[1] P. Puddu, C. Palomba, and F. Nurzia. Time-space evolution of secondary flow structures in a two-stage low-speed turbine. Number GT2006-90787. Proceedings of ASME Turbo Expo 2006: Power for Land, Sea, and Air, Spain, May 08-11 2006.

[2] L. S. Langston. Secondary flows in axial turbines—a review. *Annals of the New York Academy of Sciences*, (934):11–26, 2001.

[3] S. Kang and C. Hirsch. Three dimensional flow in a linear compressor cascade at design conditions. Number 91-GT-114. Proceedings of ASME 1991 International Gas Turbine and Aeroengine Congress and Exposition, Orlando, Florida, USA, June 03-06 1991.

[4] R. J. Goldstein and R. A. Spores. Turbulent transport on the endwall in the region between adjacent turbine blades. *ASME J. Heat Transfer*, (110):862–869, 1988.

[5] W. R. Hawthorne. Rotational flow through cascades. *Q. J. Mech. Appl. Math.*, (8(3)):266–279, 1954.

[6] R. Ciorciari, I. Kirik, and R. Niehuis. Effects of unsteady wakes on the secondary flows in the linear T106 turbine cascade. *ASME J. Turbomach.*, (136(9)), 2014.

[7] A. Krug, P. Busse, and K. Vogeler. Experimental investigation into the effects of the steady wake-tip clearance vortex interaction in a compressor cascade. *ASME J. Turbomach.*, (137(6)), 2015.

[8] R. J. Volino. Effect of unsteady wakes on boundary layer separation on a very high lift low pressure turbine airfoil. *ASME J. Turbomach.*, (134(1)), 2011.

[9] D. Lengani, D. Simoni, M. Ubaldi, P. Zunino, and F. Bertini. Time resolved PIV measurements of the unsteady wake migration in a LPT blade passage: effect of the wake passing frequency. Number ETC2017-324. Proceedings of 12th European Conference on Turbomachinery, Fluid Dynamics and Thermodynamics, ETC12, April 3-7, 2017; Stockholm, Sweden.

[10] P. Lampart. Investigation of endwall flows and losses in axial turbines. part I. formation of endwall flows and losses. *Journal of Theoretical and Applied Mechanics*, (47(2)):321–342, 2009.

[11] H. P. Hodson and R. J. Howell. The role of transition in high-lift low-pressure turbines for aeroengines. *Progress in Aerospace Sciences*, (41(6)):419–454, 2005.

[12] M. Sinkwitz, D. Engelmann, and R. Mailach. Experimental investigation of periodically unsteady wake impact on secondary flow in a 1.5 stage full annular LPT cascade with modified T106 blading. Number GT2017-64390. Proceedings of ASME Turbo Expo, Charlotte, NC, USA, June 26-30 2017.

[13] M. Berrino, D. Lengani, D. Simoni, M. Ubaldi, P. Zunino, and F. Bertini. Dynamics and turbulence characteristics of wake-boundary layer interaction in a low pressure turbine blade. Number GT2015-42626. Proceedings of ASME Turbo Expo 2015, June 15-19, Montreal, Canada.

[14] R. D. Stieger and H. P. Hodson. The transition mechanism of highly loaded low-pressure turbine blades. Number 126(4), pages 536–543, 2004.

[15] B. Winhart, M. Sinkwitz, D. Engelmann, F. di Mare, and R. Mailach. Experimental and numerical investigation of secondary flow structures in an annular LPT cascade under periodical wake impact – part 2: Numerical results. Proceedings of ISROMAC, Maui, Hawaii, December 16-21 2017.